Letter

Disentangling transport mechanisms in a correlated oxide by photoinduced charge injection

Henry Navarro,[1,*] Sarmistha Das,[1,*] Felipe Torres,[2,3,*] Rourav Basak,[1] Erbin Qiu,[1] Nicolas M. Vargas,[1,4] Pavel N. Lapa,[1,4] Ivan K. Schuller,[1,†] and Alex Frano[1,‡]

[1]*Department of Physics, Center for Advanced Nanoscience, University of California, San Diego, California 92093, USA*
[2]*Department of Physics, Universidad de Chile, Santiago 7800024, Chile*
[3]*Center for the Development of Nanoscience and Nanotechnology, CEDENNA, Santiago 9170124, Chile*
[4]*General Atomics, PO Box 85608, San Diego, California 92186, USA*

(Received 8 March 2023; accepted 30 October 2023; published 7 December 2023)

We present a novel heterostructured approach to disentangle the mechanism of electrical transport of the strongly correlated $PrNiO_3$, by placing the nickelate under the photoconductor CdS. This enables the injection of carriers into $PrNiO_3$ in a controlled way, which can be used to interrogate its intrinsic transport mechanism. We find a nonvolatile resistance decrease when illuminating the system at temperatures below the $PrNiO_3$ metal-insulator transition. The photoinduced change becomes more volatile as the temperature increases. These data help understand the intrinsic transport properties of the nickelate-CdS bilayer. Together with data from a bare $PrNiO_3$ film, we find that the transport mechanism includes a combination of mechanisms, including both thermal activation and variable range hopping. At low temperatures without photoinduced carriers, the transport is governed by hopping, while at higher temperatures and intense illumination the activation mechanism becomes relevant. This work shows a new way to control optically control the low-temperature resistance of $PrNiO_3$.

DOI: 10.1103/PhysRevMaterials.7.L123201

The electrical transport of transition metal oxides is of widespread interest because a single material can display different properties, such as metal-insulator transitions (MITs), which can be tuned by external perturbations upon slight perturbations [1–17]. Because of this tunability, focus is placed on the microscopic origin of the MITs, believing that understanding the microscopic mechanism will enable control of the electronic properties. However, for many systems, the understanding of the temperature-dependent resistance $R(T)$ is largely unexplored, ill understood, and frequently not discussed in the literature. An example of such a material is the rare-earth nickelates family ($RNiO_3$, R = rare-earth metal), a quintessential correlated oxide that displays a MIT. Since the transition is intertwined with magnetic, structural, and bond order, the origin of this transition has been a topic of intriguing debate. Ideas range from Fermi surface nesting [18,19] to a charge or bond disproportionation [20–22] and others [23]. For R = praseodymium or neodymium, a first-order MIT occurs with a paramagnetic-to-antiferromagnetic phase transition at the same temperature [9,24,25]. The transition exhibits a pronounced thermal hysteresis, typical of first-order transitions, because of the coexistence of insulating and metallic phases. Below the hysteresis, the resistance increases exponentially with decreasing temperature. Despite this behavior, seen frequently in samples from different research groups [18,26–34], the mechanism of the transport below the transition remains an open question [19–21,35–37]. Yet, interest in tuning the transport in these materials continues to grow, fueled by potential applications [28,30,38]. Possibly the lack of understanding of the transport is related to the effect of defects and sample-dependent details that do not carry over reliably from sample to sample. A methodology to investigate the transport of a single sample under variable, controlled conditions would alleviate this difficulty.

Here we outline a method to investigate the transport properties of $PrNiO_3$ (PNO), comparing transport regimes in a single sample. We designed a heterostructure that allows us to inject carriers and thus affect its transport properties in controlled way [39,40]. We place a thin film of PNO in proximity to the photoconducting CdS, which acts a source of photoinduced charge carriers [41]. While PNO does not have any response to visible light, when the heterostructure is illuminated with white light its low-temperature resistance drops by a factor of ten, allowing one to explore intrinsic transport properties of the insulating phase of the nickelate. This effect only manifests below the hysteretic regime of the first-order MIT, tying its relevance to the intrinsic ground-state properties of PNO. The phenomenology was explored experimentally as a function of light intensity, which is proportional to the number of carriers induced into the nickelate layer. Moreover, the heterostructure allows exploration of the temporal dynamics of the carriers, which are found to be long lasting, or nonvolatile, at low temperatures. As the temperature increases and approaches the hysteresis range, the photoinduced changes continually become more volatile.

Armed with this set of experimental observations, we use a model that describes the heterostructure's temperature-dependent resistance, with and without the effect of light, as well the resistance of a bare PNO film. The model combines

*These authors contributed equally to this work.
†Corresponding author: ischuller@ucsd.edu
‡Corresponding author: afrano@ucsd.edu

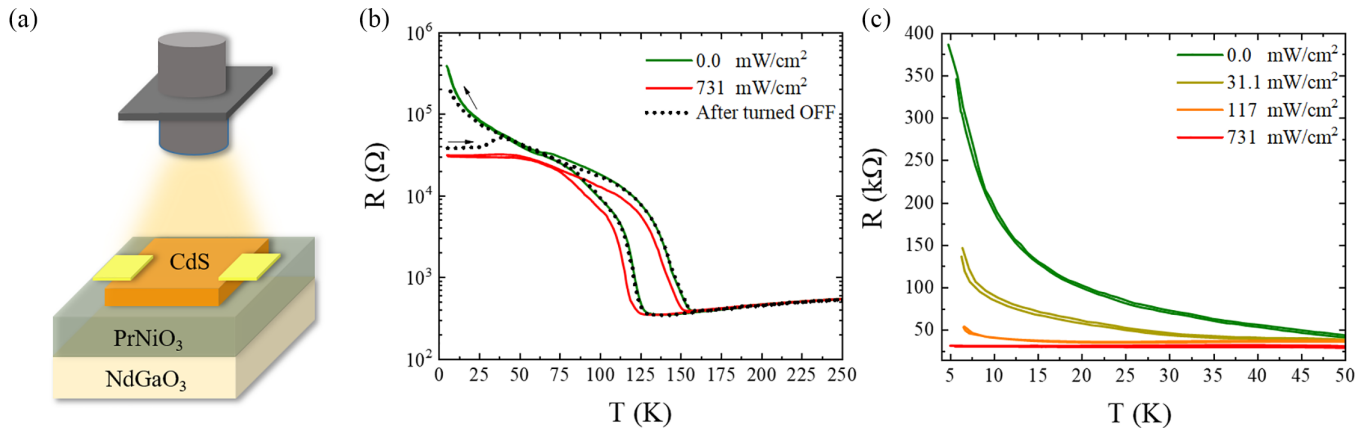

FIG. 1. (a) Experimental setup for the two-terminal (gold electrodes) resistivity and photoconductivity of the CdS-$PrNiO_3$ heterostructure. During the electrical transport measurements, a white light emitting diode was positioned over the sample. (b) Temperature dependence of the sample resistance $R(T)$ without light (green line) and with light of 731 mW/cm^2 power density turned on (red line). The black dotted curves correspond to the $R(T)$ measured in warming from 7 K after the LED is turned off. (c) $R(T)$ in the insulating state below 50 K, the temperature at which the hysteresis curves merge, measured for various light power densities.

thermally activated transport with variable range hopping (VRH) in the nickelate layer, as in previous models [36,37], but here we add the mechanism of photoinduced transport. A single model individually is insufficient, but rather a combination of the two is necessary to explain the data. At low temperatures and without light, the transport is mostly governed by hopping, while at high temperatures the thermal energy enhances the activated transport. The model then assumes that charge carriers migrate from the CdS layer into the nickelate when the light is turned on. The dependence of the resistive switching as a function of light intensity implies that at low intensity, the transport is mostly via hopping, while at high intensity the transport is mostly activated. In addition, the model also explains the nonvolatile time dependence at low temperatures and the volatile response at higher temperatures by introducing a time-dependent carrier density without any additional adjustable parameters.

Our method provides a practical tuning knob and insights into the physics of nickelates. We have developed optoelectronic control of a nickelate's resistance, which adds to the list of methodologies used to gain control of the material's resistance, such as doping, gating, pressure, and magnetic and electric fields [9,24,42–45]. This may lead to new multimodal or hybrid functionalities. In addition, in the specific case of PNO, we find that the transport is governed by both thermally activated transport and variable hopping into impurity states near the bottom of the conduction band. This is consistent with other models [18,26–28,35–37], but in our case the interplay between these two effects can be controlled by injecting charge carriers into the oxide, which is achieved through an adjacent photoconducting layer.

The hybrid device [Fig. 1(a)] was fabricated by heterostructuring PNO with a photoconducting semiconductor, CdS. An epitaxial PNO 20-nm-thick film on a single-crystal $NdGaO_3$ ⟨101⟩ substrate using pulsed laser deposition. On top of this layer, an 80-nm-thick CdS film was deposited using rf magnetron sputtering. Two gold (40-nm) electrodes were patterned on top of the CdS-PNO heterostructures. X-ray diffraction measurements were performed in a Rigaku SmartLab system at room temperature, confirming the single-phase epitaxial growth along the ⟨101⟩ direction for PNO and a polycrystalline CdS (see Supplemental Material Fig. S1 [46] for diffraction patterns). Transport measurements were carried out on a Montana C2 S50, using a Keithley 6221 current source and a Keithley 2182A nanovoltmeter. A light emitting diode (LED) with variable power density was placed over the sample, illuminating its surface [Fig. 1(a)]. In this geometry, light strongly affected the CdS and subsequently affected the bottom PNO layer through proximity effects. Since the resistance of bare CdS with light on is 2.5 orders of magnitude higher than the CdS-PNO bilayer (see Supplemental Material Fig. S3 [46] for electrical transport measurements), we consider the measured transport is through the nickelate.

Figure 1 summarizes one central finding of our work: the observation of a light-induced resistive switching in nickelates. Figure. 1(b) shows the changes in the resistance versus temperature $R(T)$ of the CdS-PNO hybrid when illuminated by the LED. Without illumination [green curves in Fig. 1(b)], the CdS-PNO hybrid exhibits a first-order MIT at around 137 K, as has been commonly observed [31,47–50]. The resistance shows a change of approximately three orders of magnitude near the hysteretic phase transition, and has a nonlinear temperature dependence in the insulating state (7 to 50 K). Upon illumination of the heterostructure with 731 mW/cm^2 white light [red curve in Fig. 1(b)], the 7 K resistance drops by a factor of approximately ten. The downward shift of the entire $R(T)$ curve indicates a slight ($\sim$ 6 K) heating by the light. However, this thermal shift is not large enough to account for the light-induced change in the low-temperature (7 K) resistance. The resistance change would be equivalent to a temperature increase from 7 K to 50 K.

After turning off the white LED [dotted lines in Fig. 1(b)], the resistance of PNO increases slightly in the insulating state (7 to 50 K). When heating after turning off the light, the resistance recovers its original value at around 50 K, which is where the heating and cooling curves merge. In Fig. 1(c), we plot $R(T)$ below 50 K for various LED fluences. With increasing fluence, the resistance decreases until it saturates

at our maximum power density, which is also evident in the normalized resistance as a function of power density and in the current-voltage curves (see Supplemental Material Fig. S2, inset [46], for power density dependence).

The nonvolatile resistance changes at low temperature described next is another key aspect of our work. Figure 2 displays the photoexcited relaxation dynamics of the PNO resistance in three-time regimes: when the light is off, $0 \leqslant t < t_{ON}$; when we shine light on the sample, $t_{ON} \leqslant t < t_{OFF}$; and after we turn off the light, $t \geqslant t_{OFF}$, with $t_{ON} = 81$ s and $t_{OFF} = 185$ s. We measured the response up to 8 hours after t_{OFF}. At lowest temperature, resistance drops quickly at t_{ON} to a value of 12% of the original resistance (ΔR_{ON}), but only recovers to about 40% of its initial state after 8 hours (ΔR_{OFF}). The only way to recover the full state of resistance is warming up the sample above the transition and cycling it back down. As the temperature increases, the light-induced resistance drops as a percentage of its initial resistance decreases, but the recovery ratio between ΔR_{OFF} and ΔR_{ON} increases. At 50 K, the transient resistance approaches the initial resistance quickly after the light is turned off, and the effect becomes volatile. This is represented in Fig. 2(c), where we plot the recovery percentage, which can be thought of as the volatility, as a function of temperature. The light-induced volatility is highest at high temperatures and becomes more nonvolatile as the temperature is lowered.

To interpret our data, we consider different models that must explain three aspects of our experimental observations (see Fig. 3). These aspects are (i) the intrinsic exponential $R(T)$ behavior of PNO below the hysteresis regime, i.e., without the effect of light; (ii) the changes in $R(T)$ upon illumination, when charge carriers migrate across the interface between CdS and PNO; and (iii) the temporal dependence of the switching behavior. In addition, we consider the $R(T)$ behavior of pure PNO, which has subtle differences compared to the heterostructure above 10 K. We also incorporate the layered architecture of the device by including the contribution of the CdS-PNO interface and the PNO resistance in a parallel configuration. The pure CdS resistance is not considered because it is one order of magnitude higher than PNO. A comparison between the pure PNO layer and CdS-PNO without light confirms the role of the CdS-PNO interface resistance even in the absence of light (Supplemental Material Fig. S4 [46] for the resistance of pure PNO).

First, we attempt to fit the data with and without light on a bare PNO film using an Arrhenius model of thermally activated transport across a gap. This yields an exponential dependence on temperature, parametrized by the activation gap E_a, written in logarithmic-scale as

$$\log(R) = \log(R_0) + \frac{E_a}{k_B T}. \quad (1)$$

While this model does not yield a good fit for the intrinsic $R(T)$, it fits increasingly better to the illuminated $R(T)$ curves with increasing power density [Fig. 3(a)]. Thus, we postulate that activation physics play a role in the photoinduced transport, but an additional mechanism is involved. Next, we evaluate variable range hopping, i.e., Mott's law, to fit the intrinsic $R(T)$ [(Fig. 3(b)]. In this model, at low temperatures, phonon-assisted tunneling of localized electrons leads to hopping conduction. As a consequence, a constant density of states close to the highest occupied energy level E_{HO} produces a temperature-dependent hopping length, henceforth called variable range hopping. Inspired by this model, we

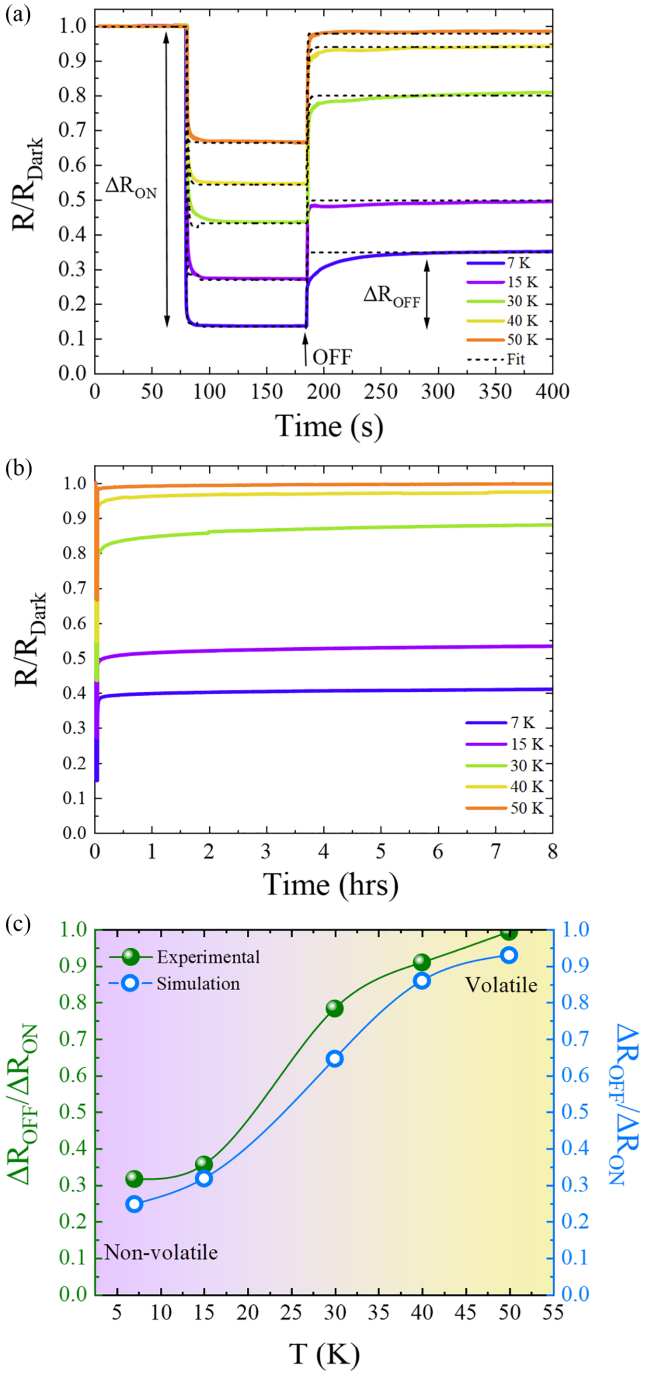

FIG. 2. (a) Time dependence of the resistance normalized to the initial insulating state before illumination taken at different temperatures: 7 K, 15 K, 30 K, 40 K, and 50 K. At $t = t_{ON} = 81$ s, the sample is illuminated, and the light is turned off at $t_{OFF} = 185$ s. The dashed black line is the fit from our model. (b) The resistance curves plotted over the span of 8 hours. (c) The ratio of resistance percentage drop when the light is turned on over the recovery percentage after the light is turned off, plotted as a function of temperature for the experimental data (green) and the model (blue).

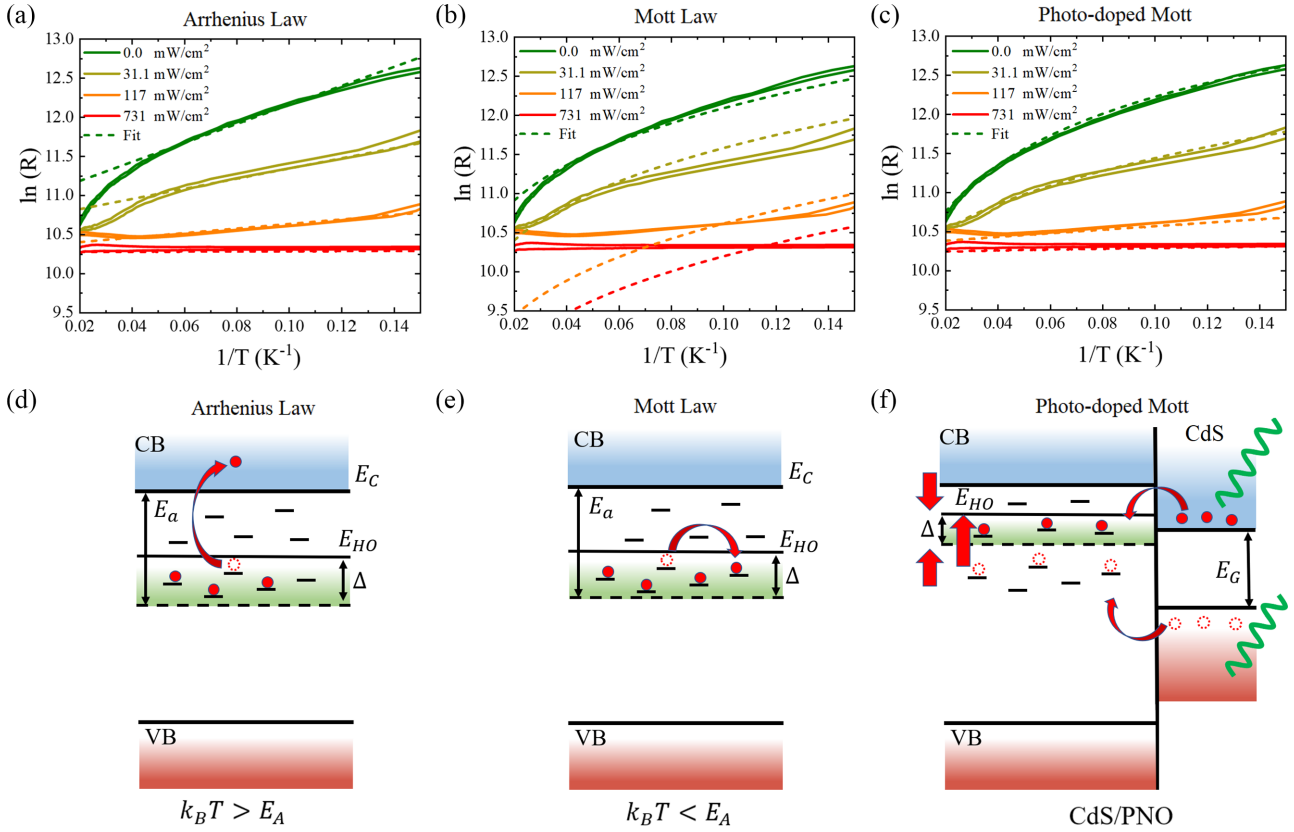

FIG. 3. The experimental $R(t)$ curves at various light power densities plotted as $\ln(R)$ as a function of $1/T$ for comparison to (a) the activated Arrhenius power law, (b) Mott's law, and (c) our phenomenological model that combines the previous two mechanisms. In the lower row, band diagrams for PNO pictorially show the effect of (d) thermal activation, (e) the Mott hopping mechanism, and (f) the photo-induced changes upon carriers entering the PNO from the CdS, shown as an adjacent band diagram. Here E_{HO} is the highest occupied energy level, E_A is the activation gap, CB is the conduction band, k_B is Boltzmann's constant, and E_G is the gap of CdS. Solid red circles are electrons and empty dotted red circles are holes

conjecture that the conduction results from hopping between shallow impurity states close to the conduction band edge ($E_{\mathrm{HO}} - \Delta$, E_{HO}), with Δ the band width below E_{HO} (see Fig. 3(e)]. The logarithmic resistance is given by [51,52]

$$\log(R) = \log(R_0) + \left(\frac{T_{\mathrm{Mott}}}{T}\right)^{1/4}, \tag{2}$$

with $T_{\mathrm{Mott}} = \frac{\beta}{k_B g(E_{\mathrm{HO}}) a^3}$, also referred to as the "Mott temperature" (for more details, see Supplemental Material [46] for conduction models). Intuitively, T_{Mott} is given by the hopping energy scale [52]. In order to avoid assumptions on the fitting parameters' dependence on increasing power, we assume that the Mott temperature is independent of light power. In this case, the fit is much better for the intrinsic $R(T)$, but starts to deviate substantially as the light power is increased [Fig. 3(b)]. Thus, the transport in the low-power regime of our measurements is mostly governed by hopping, while the high-power regime is dominated by thermal activation. When the temperature increases, we find that the Arrhenius fit degrades while the Mott law improves, suggesting that the hopping energy is greater than the thermal activation energy. For completeness, we checked different VRH models like Efros-Shklovskii and d-dimensional [53], but Mott's law is the best fitting model (see Supplemental Material Fig. S7 for conduction model fitting comparison [46]).

Inspired by the previous observations, we introduce a phenomenological model that connects continuously the intrinsic and highly photodoped conductance regimes at all temperatures. We propose that the resistivity is given by

$$\log(R) = \log(R_0) + \frac{\Delta(\Gamma) - E_a}{k_B T} + \left(\frac{T_{\mathrm{Mott}}(\Gamma)}{T}\right)^{1/4}. \tag{3}$$

The previous expression results from combining Eqs. (1) and (2), except for the inclusion of the band width Δ, which arises from considering the CdS-PNO interface effect without light. Therefore, Eq. (3) accounts for the whole range of light intensity used in our experiments. The essential feature of this model is that the band width Δ over which hopping occurs and T_{Mott} both depend on the power density Γ, as follows. As the photoinduced carriers entering the nickelate layer from the CdS fill up the states near the PNO E_{HO}, there are less impurity levels available near E_{HO}. This effectively reduces the bandwidth over which the VRH model requires the Fermi surface to have a constant density of states [see the red arrows in Fig. 3(f)]. Thus, the effective activation energy is $\Delta(\Gamma) - E_a$.

The result of these fits is shown in Fig. 3(c), revealing excellent agreement at all values of the power density across all temperatures. The values of the fitting parameters are presented in Table I, showing good agreement with

TABLE I. Fitting parameters for the photodoped Mott model.

Power Density Γ(mW/cm^2)	log(R_0)	E_a (meV)	$\Delta(\Gamma) - E_a$ (meV)	$k_B T_{\text{Mott}}(\Gamma)$ (meV)
0.0	7.3	1.03	−0.29	658.59
31.1	8.9	0.56	0.15	26.81
117	10.38	0.25	0.25	10^{-5}
731	10.28	0.01	0.02	10^{-5}

previous work [35,36,54,55]. Further, a quantitative comparison between different fitting models corroborated that our model exhibits the lowest mean squared error. Now we expand the model to study the relaxation process of the photoexcited PNO transport, where the time dependence appears naturally without any adjustable parameters. First, we consider the role of the density of charge carriers. In thermal equilibrium, the density of carriers is given by $N = n_{\text{HO}} e^{-(E_C - E_{\text{HO}})/k_B T}$, where E_C is the conduction band energy, and n_{HO} the carrier density [56]. Using $E_C - E_{\text{HO}} = E_a - \Delta$ [Fig. 3(f)] and the approximation $E_C - E_{\text{HO}} < k_B T$, we obtain a normalized carrier density given by

$$n = \frac{N - n_{\text{HO}}}{n_{\text{HO}}} = \frac{\Delta - E_a}{k_B T}. \tag{4}$$

Then, the resistance depends on the carrier density n as follows,

$$\log(R) = \log(R_0) + n + \left(\frac{T_{\text{Mott}}(\Gamma)}{T}\right)^{1/4}, \tag{5}$$

where a continuity condition governs the temporal dynamics of n,

$$\frac{dn}{dt} = \frac{n_i(\Gamma) - n}{\tau}, \tag{6}$$

where $n_i(\Gamma)$ is the initial PNO carrier concentration and τ is the relaxation time (see Supplemental Material equation S7 [46] for relaxation time). The resulting dynamics of the normalized resistance are plotted in Fig. 2 as dotted lines, showing remarkable agreement at the onset of the photoinduced switching, and good agreement when the light is turned off. Importantly, our model does not require any additional parameters to yield these fits. In addition, it captures the photoinduced effect's varying volatility as a function of temperature very well [Fig. 2(c)].

The phenomenological model can then be interpreted as follows. Electronic conduction in systems with an inhomogeneous distribution of donor levels below the conduction band is dominated by thermal excitation and hopping. The former occurs as thermally activated electrons jump to the conduction band (yielding the Arrhenius law), provided that thermal energy surpasses the activation energy. The latter is due to the electron hopping from occupied to empty donor sites. Further assumptions on the distribution of donor states gives rise to a broad range of variable range hopping models. We focus on Mott's law, which assumes that electron conduction is due to hopping between localized and uncorrelated electrons lying in a narrow, constant density-of-states band around the Fermi level.

Typically, in doped semiconductors, these two mechanisms are mutually exclusive, since the activation energy is much greater than hopping energy barrier. However, we found that in PNO, the mechanisms of thermal activation and electron hopping coexist because in PNO the activation energy and the hopping energy scales are similar. Furthermore, they can simultaneously be modified by photodoping since the injection of carriers alters the width of the band and shifts the Fermi level itself. From this, we estimate a lower threshold of the penetration depth of these photo-induced carriers, based on the idea that the transport is only feasible when the penetration depth approximates the hopping length, which we estimate at 5 nm using intrinsic parameters of PNO (see Supplemental Material [46] for hopping length details). In other words, since impurity state disorder restricts the conduction of carriers that manage to reach impurity sites, only when the dopants penetrate beyond 5 nm will they activate the transport via hopping. At low power levels (low photoinduced carrier density), the activation gap is much higher that the low (<10 K) temperature kT impeding activated transport. Thus, in this regime, the transport follows Mott's law. For $T > 10$ K, the activated and hopping mechanisms coexist. We also note that our model of intrinsic $R(T)$ at higher temperatures improves on the Mott's law fit, comparing Fig. 3(b) and 3(c) at low values of $1/T$. The Arrhenius laws becomes more relevant at higher temperatures. Also, at high power values (high photoinduced carrier density), E_A is much lower than kT throughout the whole insulating temperature regime, thus governing the activated transport. In the intermediate regimes of temperature and light power, both mechanisms contribute. As it pertains to the time relaxation, the volatility increases with temperature because the thermally activated transport is more volatile than the band structure changes that occur in the hopping regime. The changes in the band structure are more difficult to erase once the impurity states have been filled, and thus the behavior is nonvolatile when governed by hopping. Since the fit parameters obtained in our model are in good agreement with other similar works [35,36,54,55], we can conclude that the model based on the competition between thermal activation and variable range hopping is universal among nickelates.

In summary, we have developed an experimental approach to modify the resistive properties of a nickelate thin film by placing it in proximity to a photoconductor such as CdS. This approach yields a reduction in the low-temperature resistance by a factor of ten when the heterostructure is illuminated by white light. The effect is only visible below the onset of the first-order metal-to-insulator transition of the nickelate. At low temperatures, the changes are permanent, which may allow this concept to be used in technological applications

that require the encoding of memory, such as in neuromorphic devices with synaptic plasticity based on hydrogenated nickelates [57]. The volatility of the resistive changes increases as the temperature increases. To explain these data, we use a model that combines two types of transport mechanisms: thermal activation and variable range hopping. Importantly, the model captures the resistance-versus-temperature dependencies very accurately below the transition, as well as the relaxation dynamics upon switching the light on and off without any further adjustable parameters. In addition, the photoinduced method presented here may also be applied to other oxides to develop new, useful optoelectronic functionalities.

This work is based upon work supported by the National Science Foundation (Grant No. DMR-2145080) and the Air Force Office of Scientific Research [Awards No. FA9550-20-1-0242 (H.N., N.M.V., P.N.L., I.K.S.) and No. FA9550-22-1-0318]. A.F. was supported by the Research Corporation for Science Advancement via the Cottrell Scholar Award (27551) and the CIFAR Azrieli Global Scholars program.

[1] E. Dagotto, Complexity in strongly correlated electronic systems, Science **309**, 257 (2005).

[2] K. H. Ahn, T. Lookman, and A. R. Bishop, Strain-induced metal–insulator phase coexistence in perovskite manganites, Nature (London) **428**, 401 (2004).

[3] N. Vardi, E. Anouchi, T. Yamin, S. Middey, M. Kareev, J. Chakhalian, Y. Dubi, and A. Sharoni, Ramp-reversal memory and phase-boundary scarring in transition metal oxides, Adv. Mater. **29**, 1605029 (2017).

[4] Y. Tokura and N. Nagaosa, Orbital physics in transition-metal oxides, Science **288**, 462 (2000).

[5] J. Zaanen, G. A. Sawatzky, and J. W. Allen, Band gaps and electronic structure of transition-metal compounds, Phys. Rev. Lett. **55**, 418 (1985).

[6] Y. Tokura, Correlated-electron physics in transition-metal oxides, Phys. Today **56**(7), 50 (2003).

[7] B. Keimer, S. A. Kivelson, M. R. Norman, S. Uchida, and J. Zaanen, From quantum matter to high-temperature superconductivity in copper oxides, Nature (London) **518**, 179 (2015).

[8] A. P. Ramirez, Colossal magnetoresistance, J. Phys. Condens. Matter **9**, 8171 (1997).

[9] S. Middey, J. Chakhalian, P. Mahadevan, J. W. Freeland, A. J. Millis, and D. D. Sarma, Physics of ultrathin films and heterostructures of rare-earth nickelates, Annu. Rev. Mater. Res. **46**, 305 (2016).

[10] R. M. Wentzcovitch, W. W. Schulz, and P. B. Allen, VO_2: Peierls or Mott-Hubbard? A view from band theory, Phys. Rev. Lett. **72**, 3389 (1994).

[11] R. Rocco, J. del Valle, H. Navarro, P. Salev, I. K. Schuller, and M. Rozenberg, Exponential escape rate of filamentary incubation in Mott spiking neurons, Phys. Rev. Appl. **17**, 024028 (2022).

[12] S. Cheng, M.- H. Lee, R. Tran, Y. Shi, X. Li, H. Navarro, C. Adda, Q. Meng, L.- Q. Chen, R. C. Dynes, S. P. Ong, I. K. Schuller, and Y. Zhu, Inherent stochasticity during insulator-metal transition in VO_2, Proc. Natl. Acad. Sci. USA **118**, e2105895118 (2021).

[13] E. Qiu, P. Salev, L. Fratino, R. Rocco, H. Navarro, C. Adda, J. Li, M.- H. Lee, Y. Kalcheim, M. Rozenberg, and I. K. Schuller, Stochasticity in the synchronization of strongly coupled spiking oscillators, Appl. Phys. Lett. **122**, 094105 (2023).

[14] C. Ahn, A. Cavalleri, A. Georges, S. Ismail-Beigi, A. J. Millis, and J.- M. Triscone, Designing and controlling the properties of transition metal oxide quantum materials, Nat. Mater. **20**, 1462 (2021).

[15] D. Lee, B. Chung, Y. Shi, G.-Y. Kim, N. Campbell, F. Xue, K. Song, S.-Y. Choi, J. P. Podkaminer, T. H. Kim, P. J. Ryan, J.-W. Kim, T. R. Paudel, J.-H. Kang, J. W. Spinuzzi, D. A. Tenne, E. Y. Tsymbal, M. S. Rzchowski, L. Q. Chen, J. Lee, and C. B. Eom, Isostructural metal-insulator transition in VO_2, Science **362**, 1037 (2018).

[16] P. Homm, M. Menghini, J. W. Seo, S. Peters, and J.-P. Locquet, Room temperature Mott metal–insulator transition in V_2O_3 compounds induced via strain-engineering, APL Mater. **9**, 021116 (2021).

[17] E. Qiu, P. Salev, F. Torres, H. Navarro, R. C. Dynes, and I. K. Schuller, Stochastic transition in synchronized spiking nanooscillators, Proc. Natl. Acad. Sci. USA **120**, e2303765120 (2023).

[18] R. S. Dhaka, T. Das, N. C. Plumb, Z. Ristic, W. Kong, C. E. Matt, N. Xu, K. Dolui, E. Razzoli, M. Medarde, L. Patthey, M. Shi, M. Radović, and J. Mesot, Tuning the metal-insulator transition in $NdNiO_3$ heterostructures via Fermi surface instability and spin fluctuations, Phys. Rev. B **92**, 035127 (2015).

[19] S. Lee, R. Chen, and L. Balents, Landau theory of charge and spin ordering in the nickelates, Phys. Rev. Lett. **106**, 016405 (2011).

[20] M. Medarde, C. Dallera, M. Grioni, B. Delley, F. Vernay, J. Mesot, M. Sikora, J. A. Alonso, and M. J. Martínez-Lope, Charge disproportionation in $R$$NiO_3$ perovskites (R = rare earth) from high-resolution x-ray absorption spectroscopy, Phys. Rev. B **80**, 245105 (2009).

[21] R. J. Green, M. W. Haverkort, and G. A. Sawatzky, Bond disproportionation and dynamical charge fluctuations in the perovskite rare-earth nickelates, Phys. Rev. B **94**, 195127 (2016).

[22] B. Lau and A. J. Millis, Theory of the magnetic and metal-insulator transitions in $R$$NiO_3$ bulk and layered structures, Phys. Rev. Lett. **110**, 126404 (2013).

[23] H. Park, A. J. Millis, and C. A. Marianetti, Site-selective Mott transition in rare-earth-element nickelates, Phys. Rev. Lett. **109**, 156402 (2012).

[24] M. H. Upton, Y. Choi, H. Park, J. Liu, D. Meyers, J. Chakhalian, S. Middey, J.- W. Kim, and P. J. Ryan, Novel electronic behavior driving $NdNiO_3$ metal-insulator transition, Phys. Rev. Lett. **115**, 036401 (2015).

[25] M. Medarde, M. T. Fernández-Díaz, and P. Lacorre, Long-range charge order in the low-temperature insulating phase of $PrNiO_3$, Phys. Rev. B **78**, 212101 (2008).

[26] J. Y. Zhang, H. Kim, E. Mikheev, A. J. Hauser, and S. Stemmer, Key role of lattice symmetry in the metal-insulator transition of $NdNiO_3$ films, Sci. Rep. **6**, 23652 (2016).

[27] X. K. Lian, F. Chen, X. L. Tan, P. F. Chen, L. F. Wang, G. Y. Gao, S. W. Jin, and W. B. Wu, Anisotropic-strain-controlled metal-insulator transition in epitaxial $NdNiO_3$ films grown

on orthorhombic $NdGaO_3$ substrates, Appl. Phys. Lett. **103**, 172110 (2013).

[28] D. Preziosi, L. Lopez-Mir, X. Li, T. Cornelissen, J. H. Lee, F. Trier, K. Bouzehouane, S. Valencia, A. Gloter, A. Barthélémy, and M. Bibes, Direct mapping of phase separation across the metal–insulator transition of $NdNiO_3$, Nano Lett. **18**, 2226 (2018).

[29] A. S. Disa, D. P. Kumah, J. H. Ngai, E. D. Specht, D. A. Arena, F. J. Walker, and C. H. Ahn, Phase diagram of compressively strained nickelate thin films, APL Mater. **1**, 032110 (2013).

[30] G. Mattoni, P. Zubko, F. Maccherozzi, A. J. H. van der Torren, D. B. Boltje, M. Hadjimichael, N. Manca, S. Catalano, M. Gibert, Y. Liu, J. Aarts, J. M. Triscone, S. S. Dhesi, and A. D. Caviglia, Striped nanoscale phase separation at the metal–insulator transition of heteroepitaxial nickelates, Nat. Commun. **7**, 13141 (2016).

[31] J. del Valle, R. Rocco, C. Domínguez, J. Fowlie, S. Gariglio, M. J. Rozenberg, and J.- M. Triscone, Dynamics of the electrically induced insulator-to-metal transition in rare-earth nickelates, Phys. Rev. B **104**, 165141 (2021).

[32] E. Mikheev, A. J. Hauser, B. Himmetoglu, N. E. Moreno, A. Janotti, C. G. Van de Walle, and S. Stemmer, Tuning bad metal and non-Fermi liquid behavior in a Mott material: Rare-earth nickelate thin films, Sci. Adv. **1**, e1500797 (2015).

[33] A. J. Hauser, E. Mikheev, N. E. Moreno, T. A. Cain, J. Hwang, J. Y. Zhang, and S. Stemmer, Temperature-dependence of the Hall coefficient of $NdNiO_3$ thin films, Appl. Phys. Lett. **103**, 182105 (2013).

[34] J. Liu, M. Kargarian, M. Kareev, B. Gray, P. J. Ryan, A. Cruz, N. Tahir, Y.- D. Chuang, J. Guo, J. M. Rondinelli, J. W. Freeland, G. A. Fiete, and J. Chakhalian, Heterointerface engineered electronic and magnetic phases of $NdNiO_3$ thin films, Nat. Commun. **4**, 2714 (2013).

[35] Q. Guo, S. Farokhipoor, C. Magén, F. Rivadulla, and B. Noheda, Tunable resistivity exponents in the metallic phase of epitaxial nickelates, Nat. Commun. **11**, 2949 (2020).

[36] G. Catalan, R. M. Bowman, and J. M. Gregg, Metal-insulator transitions in $NdNiO_3$ thin films, Phys. Rev. B **62**, 7892 (2000).

[37] R. Mallik, E. V. Sampathkumaran, J. A. Alonso, and M. J. Martinez-Lope, Complex low-temperature transport behaviour of $R NiO_3$-type compounds, J. Phys. Condens. Matter **10**, 3969 (1998).

[38] A. M. Alsaqqa, S. Singh, S. Middey, M. Kareev, J. Chakhalian, and G. Sambandamurthy, Phase coexistence and dynamical behavior in $NdNiO_3$ ultrathin films, Phys. Rev. B **95**, 125132 (2017).

[39] H. Navarro, J. d. Valle, Y. Kalcheim, N. M. Vargas, C. Adda, M.- H. Lee, P. Lapa, A. Rivera-Calzada, I. A. Zaluzhnyy, E. Qiu, O. Shpyrko, M. Rozenberg, A. Frano, and I. K. Schuller, A hybrid optoelectronic Mott insulator, Appl. Phys. Lett. **118**, 141901 (2021).

[40] C. Adda, H. Navarro, J. Kaur, M.- H. Lee, C. Chen, M. Rozenberg, S. P. Ong, and I. K. Schuller, An optoelectronic heterostructure for neuromorphic computing: CdS/V_3O_5, Appl. Phys. Lett. **121**, 041901 (2022).

[41] H. Navarro, A. C. Basaran, F. Ajejas, L. Fratino, S. Bag, T. D. Wang, E. Qiu, V. Rouco, I. Tenreiro, F. Torres, A. Rivera-Calzada, J. Santamaria, M. Rozenberg, and I. K. Schuller, Light-induced decoupling of electronic and magnetic properties in manganites, Phys. Rev. Appl. **19**, 044077 (2023).

[42] S. Catalano, M. Gibert, J. Fowlie, J. Íñiguez, and J. M. Triscone, and J. Kreisel, Rare-earth nickelates $R NiO_3$: Thin films and heterostructures, Rep. Prog. Phys. **81**, 046501 (2018).

[43] S. D. Ha, U. Vetter, J. Shi, and S. Ramanathan, Electrostatic gating of metallic and insulating phases in $SmNiO_3$ ultrathin films, Appl. Phys. Lett. **102**, 183102 (2013).

[44] R. Scherwitzl, P. Zubko, I. G. Lezama, S. Ono, A. F. Morpurgo, G. Catalan, and J.- M. Triscone, Electric-field control of the metal-insulator transition in ultrathin $NdNiO_3$ films, Adv. Mater. **22**, 5517 (2010).

[45] S. Asanuma, P.- H. Xiang, H. Yamada, H. Sato, I. H. Inoue, H. Akoh, A. Sawa, K. Ueno, H. Shimotani, H. Yuan, M. Kawasaki, and Y. Iwasa, Tuning of the metal-insulator transition in electrolyte-gated $NdNiO_3$ thin films, Appl. Phys. Lett. **97**, 142110 (2010).

[46] See Supplemental Material at http://link.aps.org/supplemental/10.1103/PhysRevMaterials.7.L123201 for conduction models and additional electrical transport measurement.

[47] X. Granados, J. Fontcuberta, X. Obradors, and J. B. Torrance, Metastable metallic state and hysteresis below the metal-insulator transition in $PrNiO_3$, Phys. Rev. B **46**, 15683 (1992).

[48] M. Hepting, M. Minola, A. Frano, G. Cristiani, G. Logvenov, E. Schierle, M. Wu, M. Bluschke, E. Weschke, H.-U. Habermeier, E. Benckiser, M. Le Tacon, and B. Keimer, Tunable charge and spin order in $PrNiO_3$ thin films and superlattices, Phys. Rev. Lett. **113**, 227206 (2014).

[49] M. A. Novojilov, O. Y. Gorbenko, I. E. Graboy, A. R. Kaul, H. W. Zandbergen, N. A. Babushkina, and L. M. Belova, Perovskite rare-earth nickelates in the thin-film epitaxial state, Appl. Phys. Lett. **76**, 2041 (2000).

[50] M. S. Saleem, C. Song, F. Li, Y. Gu, X. Chen, G. Shi, Q. Li, X. Zhou, and F. Pan, Light tuning of the resistance of $NdNiO_3$ films with $CoFe_2O_4$ capping, Physica Status Solidi Rapid Res. Lett., **12**, 1800186 (2018).

[51] B. I. Shklovskii and A. L. Efros, *Electronic Properties of Doped Semiconductors* (Springer-Verlag, Berlin, 1984).

[52] N. F. Mott, Conduction in glasses containing transition metal ions, J. Noncryst. Solids **1**, 1 (1968).

[53] A. L. Efros and B. I. Shklovskii, Coulomb gap and low temperature conductivity of disordered systems, J. Phys. C Solid State Phys. **8**, L49 (1975).

[54] S. Harisankar, K. Soni, E. Yadav, and K. R. Mavani, Strain-mediated effects of oxygen deficiency and variation in non-Fermi liquid behavior of epitaxial $PrNiO_{3-\delta}$ thin films, J. Phys. Condens. Matter **31**, 135601 (2019).

[55] K. Ramadoss, N. Mandal, X. Dai, Z. Wan, Y. Zhou, L. Rokhinson, Y. P. Chen, J. Hu, and S. Ramanathan, Sign reversal of magnetoresistance in a perovskite nickelate by electron doping, Phys. Rev. B **94**, 235124 (2016).

[56] D. A. Neamen, *Semiconductor Physics and Devices: Basic Principles*, 4th ed. (McGraw-Hill Higher Education, New York, 2012).

[57] H.- T. Zhang *et al.*, Perovskite neural trees, Nat. Commun. **11**, 2245 (2020).